Synthesis of Liposome-Templated Titania Nanodisks: Optical Properties and Photocatalytic Activities

Minjoong Yoon,* Mijung Seo, Cheoljin Jeong, Joon Hee Jang, and Ki Seok Jeon†

Molecular/Nano Photochemistry and Photonics Lab, Department of Chemistry, Chungnam National University, Daejeon 305-764, Korea

Received July 20, 2005. Revised Manuscript Received September 21, 2005

New spherical nanostructures of titania (TiO_2) have been synthesized through formation of liposome−TiO_2 nanocomposites by using egg lecithin lipid as a template, and their optical properties have been investigated with regard to the dynamics of surface charge carriers and photocatalytic activities by using UV−vis and photoluminescence (PL) spectroscopic techniques. On the basis of the measurements of X-ray diffraction, transmission electron microscopy, and atomic force microscopy, the spherical titania nanostructures are identified to be anatase crystalline nanodisks with an average diameter of 9 nm and height of 0.5 nm. The nanodisks have a large Brunauer−Emmett−Teller specific surface area of 227 m^2/g. The FT-IR and X-ray photoemission spectra of the nanodisks confirm that the skeleton structure of the titania nanodisk is formed through H-bonding of the −Ti−O−Ti− network through tetrahedrally coordinated vacancies designated $_4Ti^{4+}$−OH. Analysis of the UV−vis and PL spectra reveals that the band-gap energy is red-shifted to 3.02 eV from that of TiO_2 nanoparticle dots and its transition nature is exclusively indirect. The PL emission spectrum of the titania nanodisks exhibits a strong structural emission band around 420 nm with shoulders around 470 and 550 nm which is attributed to the transition from three different exciton-trapped surface states. In addition, another surface emission originating from the coordinatively unsaturated ions (Ti^{3+}) is observed at 618 nm. These results suggest that coupling of the surface charge carriers with the lattice phonon of the nanostructures is so strong that the dominant route to charge recombination in titania nanodisks is nonradiative. Supporting the steady-state spectral observations, the decay profiles of the surface emission measured by using a femtosecond laser time-resolved PL system fit into a triexponential function with relatively longer lifetimes (20−30 ps, 1.1−1.5 ns, and 4.5−6.0 ns) as compared to those of simple nanoparticle dots, indicating that recombination of the charge carriers on the nanodisk surface is very prolonged. Being consistent with this, the photocatalytic efficiency for the reduction of methyl orange is much higher in the presence of the titania nanodisks than that observed in the presence of Degussa P-25.

Introduction

Titania (TiO_2) nanoparticles have been attracting a great deal of attention due to their potential applications in developing photocatalysts, photoelectronic devices, and sensors.[1−3] Because these applications are based on the photogeneration of charge carriers such as electrons and holes, success in the applications of titania nanoparticles relies on the electron or hole transfer efficiency, which is dependent on the recombination dynamics of the photogenerated surface charge carriers. Therefore, to improve the photoelectrical function of the titania nanoparticles, it is important to control the recombination dynamics of the photogenerated charge carrier on the surface. The recombination dynamics of the nanoparticles used to be controlled by tailoring the particle size. For example, as the particle size is smaller than the thickness of the space charge layer, the Brunauer−Emmett−Teller (BET) specific surface area is larger, and separation between the electron and hole wave functions is effective so that the recombination is retarded. Alternatively, the recombination dynamics can be controlled by surface modification through incorporation of the nanoparticles with some supporters such as zeolites and Vyco glass.[4−7] However, in the case of nanoparticles such as quantum dots, these controlling methods remain limited to increase the BET specific surface area to further improve the efficiency of photogenerated charge-carrier transfer. Therefore, the use of higher dimensional single-crystal nanostructures such as nanotubes, nanoballs, or nanorods with a quite high aspect ratio and a large BET specific surface area would be one promising option, because the intercrystalline contacts can be highly decreased so that the charge-carrier transfer is facilitated through the lattice layer.

In the synthetic direction of new nanostructures based on ordered assembly of nanocrystals, two significant factors are

* To whom correspondence should be addressed. E-mail: mjyoon@cnu.ac.kr.
† Present address: Department of Chemistry, Kongju National University, Kongju, Chungnam 314-701, Korea.

(1) Yoon, M.; Chang, J. A.; Kim, Y.; Choi, J. R.; Kim, K.; Lee, S. J. *J. Phys. Chem. B* **2001**, *105*, 2539.
(2) O'Regan, B.; Moser, J.; Anderson, M.; Gratzel, M. *J. Phys. Chem.* **1990**, *94*, 8720.
(3) Varlan, A. R.; Suls, J.; Sansen, W.; Veelaert, D.; Loof, A. D. *Sens. Actuators, B* **1997**, *44*, 334.
(4) Corrent, S.; Cosa, G.; Scaiano, J. C.; Galletero, M. S.; Alvaro, M.; Garcia, H. *Chem. Mater.* **2001**, *13*, 715.
(5) Anandan, S.; Yoon, M. *J. Photochem. Photobiol., C* **2003**, *4*, 5.
(6) Anpo, M.; Aikawa, N.; Kubokawa, Y. *J. Phys. Chem.* **1985**, *89*, 5017.
(7) Matthews, R. W. *J. Phys. Chem.* **1988**, *92*, 6853.

10.1021/cm0515855 CCC: $30.25
Published on Web 10/25/2005

important, namely, their shape and size distribution, influencing the physical properties of the nanostructures. To control these factors, the self-assembled molecule has been used as a template to construct metallic and semiconductor nanostructures. The most popular self-assembled molecule has been a surfactant forming micelles. Recently, single-crystalline titania nanotubes have been synthesized by the Adachi group[8−10] by using a surfactant, laurylamine hydrochloride. It has been successfully applied to develop a highly efficient photocatalyst and dye-sensitized solar cell,[11] and its photoelectrical efficiencies are much higher than those of other titania nanotubes prepared by Hoyer[12] and Kasuga et al.[13] It should be noted that Kasuga's titania nanotubes have a much higher BET specific surface area (400 m^2/g) than Adachi's nanotubes, implying that, in addition to the particle size effect, the morphological effects on the photon-to-electron conversion efficiency of the titania nanotubes are also important.

In relation to the dynamics of the surface charge carriers of titania nanoparticles, time-resolved diffuse reflectance spectroscopy[14,15] and time-resolved microwave conductivity[16,17] have been mostly studied. In addition to these methods, time-resolved photoluminescence (PL) spectroscopy is also useful, but very few reports have addressed the time-resolved PL properties[18,19] of titania nanoparticles despite many reports of steady-state PL properties. Furthermore, these PL studies have been limited to tinania nanoparticle dots, and the PL properties of the titania nanostructures, particularly their morphology dependence, have not been systematically investigated. Thus, it is worthwhile to synthesize different types of titania nanostructures and investigate their PL properties to determine their morphology effects on the dynamics of the surface charge carriers.

In the present work, new spherical titania nanostructures such as nanodisks were synthesized through formation of liposome−TiO_2 nanocomposites by using egg lecithin lipid as a template, followed by characterization of their structure and sizes by using X-ray diffraction (XRD), transmission electron microscopy (TEM), atomic force microscopy (AFM), Fourier transform infrared (FT-IR) spectrometry, and X-ray photoelectron spectrometry (XPS). Thereafter, their steady-state and time-resolved PL properties were investigated, being related to the excited-state dynamics of surface charge carriers. The photocatalytic activity of titania nanodisks was also measured and discussed in terms of the dynamics of surface charge carriers by comparison with that of Degussa P-25.

Experimental Section

Materials. The chemicals for the synthesis of titania nanoparticles, titanium(IV) isopropoxide (99.999%, Aldrich), egg lecithin (L-α-phosphatidylcholine, >60%, Aldrich), chloroform (>99.8%, Merck), and 2-propanol (>99.9%, Merck), were used as received. As a precursor to the synthesis of the titania nanostructures, TiO_2 nanoparticle colloids (average size ∼9 nm in diameter) were prepared via a hydrolysis method using titanium(IV) isopropoxide under the condition of pH 1.5 adjusted with HCl according to the previously reported procedures.[20]

Synthesis of Liposome-Templated Titania Nanodisks. The titania nanodisks were synthesized by forming molecular assembled unilamellar lipid vesicle (liposome)−TiO_2 nanocomposites. At first, to form the liposome−TiO_2 nanocomposites, a thin phospholipid film was prepared by evaporating a chloroform solution of egg lecithin lipid (0.025 g/mL) to dryness in a round-bottom flask under reduced pressure. The lipid films were mixed with a 2% TiO_2 nanoparticle colloidal solution (150 mL), followed by sonication for 60 min in an ultrasonic bath (Fisher Scientific model FS20, 70 W, 42 kHz), to produce turbid liposome−TiO_2 composites. The turbid solution of liposome−TiO_2 composites was centrifuged at 4500 rpm for 30 min by using an ultracentrifuge, and the transparent supernatant solution, which is supposed to contain a homogeneous distribution of liposome−TiO_2 nanocomposites, was separated from the sedimented particles. The transparent supernatant solution was gelled by incubation at 40 °C at a humidity of 70% for 1 day. The obtained gel was freeze-dried by speed vacuum for 30 min, followed by calcinations at 823 K for 24 h in a crucible or quartz plate to remove lipids, resulting in the formation of TiO_2 fine powders.

To characterize the crystalline phase of the produced materials, XRD patterns of the sample were recorded on a Rigaku Rotaflex diffractometer (model no. D/MAX-2200 Ultima/PC, rotating Cu target, 3 kW X-ray and set to 40 kV and 40 mA) at an X-ray incident angle 0.02°. The morphology of the synthesized materials was examined by TEM (JEOL JEM-2010, Japan) and AFM (NanoScopeIIIA). Samples for TEM measurement were prepared by dip-coating Formvar/carbon film Cu grids with a nanocolloidal solution obtained by sonicating the produced powder material in ethanol. On the other hand, AFM images were measured in tapping mode with samples prepared by calcinations of the liposome−TiO_2 nanocomposites on a quartz plate or by drying the nanocolloidal solution on a Si wafer. The BET specific surface area was determined by measuring N_2 adsorption and desorption isotherms on a Micrometrics ASAP 2000 sorptometer at −196 °C.

Spectroscopic Measurements. Surface analysis of the synthesized titania nanostructures was performed by using FT-IR and XPS spectroscopy. The FT-IR spectra were recorded on a JASCO FT-IR spectrophotometer in the diffuse reflectance mode at a resolution of 4 cm^{-1}. The XPS spectra of the titania nanostructures were measured by using a Multilab ESCA 2000 fitted with an Mg Kα source (1253.6 eV) with two ultra-high-vacuum (UHV) chambers, one for sample preparation and the other for analysis. The anode was operated at 120 W (10 mA and 12kV), and the analyzer was operated at a constant narrow scan pass energy of 30 eV. The analysis area was 2 × 3 mm. The photoelectrons were collected at an electron takeoff angle of 55°. The binding energy shifts due to

(8) Adachi, M.; Murata, Y.; Harada, M.; Yoshikawa, S. *Chem. Lett.* **2000**, 942.
(9) Adachi, M.; Harada, T.; Harada, M. *Langmuir* **1999**, *15*, 7097.
(10) Adachi, M.; Harada, T.; Harada, M. *Langmuir* **2000**, *16*, 2376.
(11) Adachi, M.; Murata, Y.; Okada, I.; Yoshikawa, S. *J. Electrochem. Soc.* **2003**, *150*, G488.
(12) Hoyer, P. *Langmuir* **1996**, *12*, 1411.
(13) Kasuga, T.; Hiramatsu, M.; Hoson, A.; Sekino, T.; Niihara, K. *Langmuir* **1998**, *14*, 3160.
(14) Furube, A.; Asahi, T.; Masuhara, H.; Yamashita, H.; Anpo, M. *Chem. Lett.* **1997**, 735.
(15) Furube, A.; Asahi, T.; Masuhara, H.; Yamashita, H.; Anpo, M. *J. Phys. Chem. B* **1999**, *103*, 3120.
(16) Matin, S. T.; Hermann, H.; Choi, W.; Hoffmann, M. R. *J. Chem. Soc., Faraday Trans.* **1994**, *90*, 3315.
(17) Fessenden, R. W.; Kamat, P. V. *J. Phys. Chem.* **1995**, *99*, 12902.
(18) Amtout, A.; Leoneli, R. *Solid State Commun.* **1992**, *84*, 349.
(19) Fujihara, K.; Izumi, S.; Ohno, T.; Matsumura, M. *J. Photochem. Photobiol., A* **2000**, *132*, 99.
(20) Duonghong, D.; Ramsden, J.; Gratzel, M. *J. Am. Chem. Soc.* **1982**, *104*, 2977.

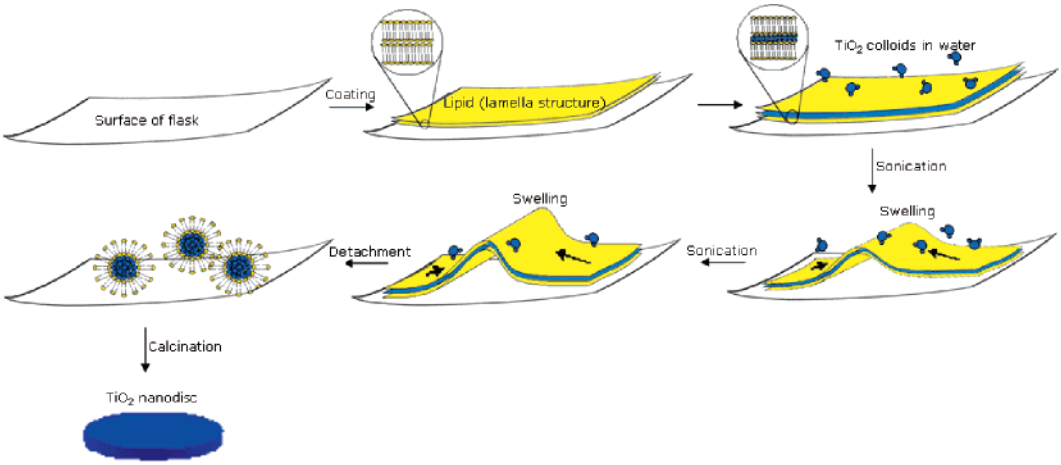

Figure 1. Schematic diagram illustrating the formation of liposome-templated TiO_2 nanocomposites as a precursor for titania nanodisks (see the text for details).

surface charging were corrected using the C 1s core level at 285 eV as an internal standard.

Diffuse reflectance UV−vis absorption spectra were recorded by using a Shimadzu UV-3101PC spectrophotometer equipped with an integral sphere.

The PL spectral measurements were made with the synthesized TiO_2 nanostructural powders (0.03 g) either coated on quartz glass or dispersed in water (10 mL) in the ultrasonic bath. Before the PL measurements, the solutions were bubbled with high-purity Ar to remove the dissolved oxygen. The steady-state PL spectra were measured on a scanning SLM-AMINCO 4800 spectrofluorometer. The time-resolved PL spectra were measured by using a time-correlated single-photon-counting (TCSPC) method.[21,22] The excitation source is a self-mode-locked Ti:sapphire laser (Coherent model Mira 900) pumped by a Nd:YVO_4 laser (Coherent Verbi diode-pumped laser). The laser output has a ~200 fs pulse width with a repetition rate of 76 MHz, and it can span the excitation wavelength in the ranges of 235−300 and 350−490 nm by second and third harmonic generations by means of LBO and BBO crystals, respectively. To avoid unexpected behavior of the excited surface states of titania, the laser pulse power was minimized to 1.2 μW/pulse by passing the laser pulse through a pulse picker. The beam area on the sample was about 1.5 mm^2. All the standard electronics for the TCSPC system were from Edinburgh Instruments. The instrument function was measured by detecting a scattered laser pulse of ~200 fs with a quartz crystal. This system allows a time resolution of ca. 2 ps after deconvolution. The PL decays were analyzed to fit exponential functions following a deconvolution procedure, using a proper instrument response function. The goodness of the fits was judged from the reduced χ^2 values and the distribution of the weighted residuals among the data channels.[22] For all the accepted fits, the χ^2 values were within 1.00−1.20, and the weighted residuals were randomly distributed among the data channels used. For all the PL spectral measurements, the scattered excitation light was eliminated using color glass filters (HOYA, L-37 and L-39).

Measurement of Photocatalytic Activities. Photocatalytic activities of the TiO_2 nanodisks as well as Degussa P-25 were measured by monitoring photoreduction of methyl orange (MO) in aqueous solution containing the photocatalysts. A 5 mg portion of TiO_2 nanodisks or Degussa-P-25 was mixed with 10 mL of the aqueous MO solution (5×10^{-6} M) in optically matched Pyrex test tubes, and the mixed solutions were simultaneously irradiated in the Rayonet UV−photochemical reactor (Southern New England Ultraviolet Co.) under argon gas flow, which allows photoreduction only via electron transfer from TiO_2 as well as mixing of the heterogeneous solutions containing the photocatalysts. After a certain period of irradiation, each solution was centrifuged to sediment the photocatalysts, followed by taking the supernatant solution to measure the absorption spectral change of MO to monitor the photoreduction. Similarly, the photocatalytic oxidation of MO in the aqueous solution was also measured under mild oxygen bubbling conditions during irradiation. The power of the irradiation lamp was determined to be 9.7×10^{-9} einstein/min by the actinometric method.

Results and Discussion

Formation and Characterization of Titania Nanodisks. The formation mechanism of titania nanodisks is not unambiguously understood at present. Nevertheless, on the basis of a known formation mechanism of lipid vesicles,[23] we could propose the formation process of the titania nanodisks as shown in Figure 1. The thin phospholipid film attached to the glass of the round-bottom flask is known to have the appearance of concentric domelike lamellae.[23] Addition of the TiO_2 nanoparticle colloidal solution over the lipid film resulted in gradual swelling through interaction with the TiO_2 colloids in the intra-lipid bilayer. Mild sonication causes further swelling, detachment of the lamellae containing TiO_2 from the surface of the glass, and curling up of the lamellae into predominantly unilamallar liposome−TiO_2 composites of heterogeneous size distribution. Ultracentrifugation of the heterogeneous liposome−TiO_2 composites resulted in separation of the transparent solution from the large liposome−TiO_2 composites. The transparent solution was found to contain more or less homogeneous liposome−TiO_2 nanocomposites smaller than the light wavelength as confirmed by observing the TEM images. The transparent solution was gelled by incubation at 40 °C at a humidity of 70% for 24 h. The liposome−TiO_2 nanocomposite powders obtained by freeze-drying of the gel were amorphous as determined from their broad and unresolved XRD peaks (Figure 2). However, the calcinations of the

(21) O'Conner, D. V.; Phillips, D. *Time Correlated Single Photon Counting*; Academic Press: New York, 1984.
(22) Kim, Y.; Yoon, M.; Kim, D. *J. Photochem. Photobiol., A* **2001**, *138*, 167.
(23) Fendler, J. H. *Membrane Mimetic Chemistry*; John Wiley & Sons: New York, 1982.

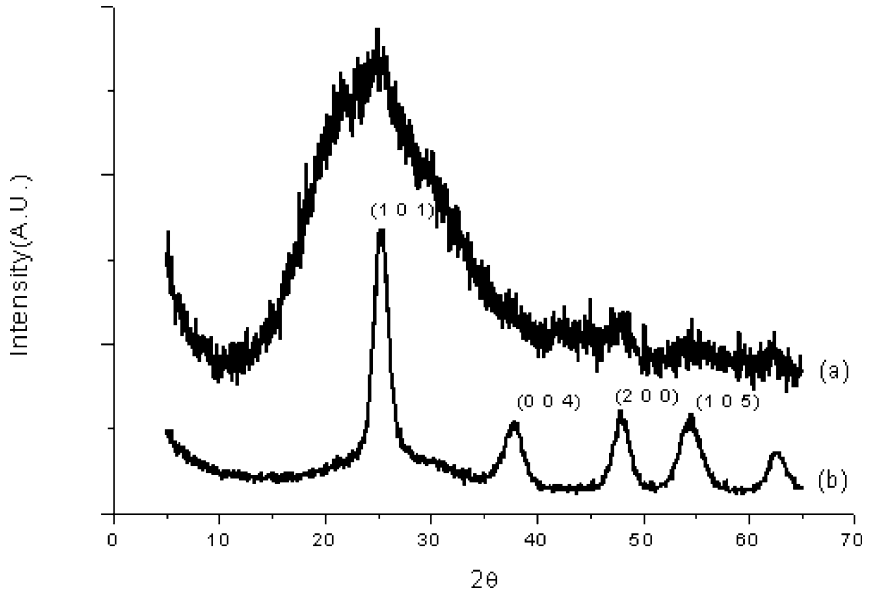

Figure 2. X-ray diffraction patterns of (a) liposome−TiO_2 nanocomposites and (b) single-crystalline titania nanocrystals.

amorphous liposome−TiO_2 composites resulted in the formation of single-crystalline titania fine powders as demonstrated by their sharply resolved XRD peaks corresponding to the (101), (004), (200), and (105) crystal faces of anatase.[24] This indicates that the titania fine powders obtained here are single crystals of anatase. It is interesting to note that their XRD peaks are still not so sharp as compared to the highly crystalline bulk titania or standard titania nanoparticles P-25. This must be attributed to the smaller size of the fine powders prepared in this work as compared to that of the P-25 (mean crystalline size ~30 nm).[24] Actually, the Debye−Scherrer analysis of the line width of the (101) reflection determined the size of the crystalline domains was about 9 nm.[25]

These fine powders were dispersed in ethanol by sonication, and the suspension was dropped onto a perforated carbon grid. After drying, the powders were observed by TEM at an accelerating voltage of 220 V. Figure 3A shows the TEM image of the titania powders, exhibiting a spherical shape, though there was considerable distribution in size as shown in Figure 3B. Many particles exhibited irregular shapes and sizes, but these distributions depended on aggregation of the small particles during the TEM sample preparation. Nevertheless, their crystalline perfection was high as demonstrated by the observation of the selected-area electron diffraction (SAED) pattern showing the Debye−Sherrer rings corresponding to the diffractions of the anatase phase as interpreted from the XRD patterns. The good crystalline character of the titania nanospherical particle was also confirmed by observation of lattice images with high-resolution TEM (HRTEM) as shown in Figure 3C. The observed lattice spacing as shown in the inset of Figure 3C was observed to be about 0.35 nm, close to the anatase 101 cell spacing.[26] The average particle size observed from the TEM image is about 10 nm in diameter, which appeared in general agreement with that determined from the XRD reflection line width (vide supra). It is noteworthy that the diameter size of the present liposome-templated titania nanoparticle is similar to that of the TiO_2 nanoparticle prepared by the hydrolysis method, implying that the TEM image is not enough to identify the morphology of the liposome-templated nanoparticles.

To observe the morphology of the liposome-templated nanoparticles more specifically, tapping-mode AFM was performed by using samples prepared by calcinations of the liposome−TiO_2 nanocomposites on a quartz plate; the freeze-dried liposome−TiO_2 nanocomposite powders were dispersed in ethanol in the ultrasonic bath, and the suspension was dropped onto a quartz glass plate followed by calcinations at 825 K for 24 h. Figure 4 illustrates 500 nm × 500 nm images of the titania nanospherical particles formed on the quartz glass plate. The size distribution seems to be the same as that observed from TEM images, exhibiting that the average particle size is ca. 9 nm in diameter and ca. 0.5 nm in height. Such AFM images were very similar to those measured by using the samples prepared by coating a Si wafer with the titania nanospherical powders redispersed in ethanol. These results confirm that the nanospherical particles are actually two-dimensional nanodisk structures with a high aspect ratio (ca. 18) which are supposed to have a large specific surface area.[13] Actually, the BET specific surface area of titania nanodisks was determined to be 227 m^2/g by using the N_2 adsorption isotherm technique, which is rather large as anticipated for other titania nanostructures such as nanotubes having high photocatalytic activities.[11]

Figure 5 shows the FT-IR spectra of the titania nanodisks as well as the TiO_2 nanoparticles prepared by the hydrolysis method. Four different regions of characteristic bands were observed for the titania nanodisks (curve a) in contrast to two regions observed for the TiO_2 nanoparticles (curve b). The region of 500−900 cm^{-1} showing the rather weak and broad features is identified to be the Ti−O stretching vibrational frequency region.[27] A broad band around 3400

(24) Serpone, N.; Lawless, D.; Khairutdinov, R. *J. Phys. Chem.* **1995**, *99*, 16646.
(25) Cullity, B. D. *Elements of X-ray Diffraction*, 2nd ed.; Addison-Wesley: Reading, MA, 1978.
(26) Wang, Y. Q.; Hu, G. Q.; Duan, X. F.; Sun, H. L.; Xue, Q. K. *Chem. Phys. Lett.* **2002**, *365*, 427.

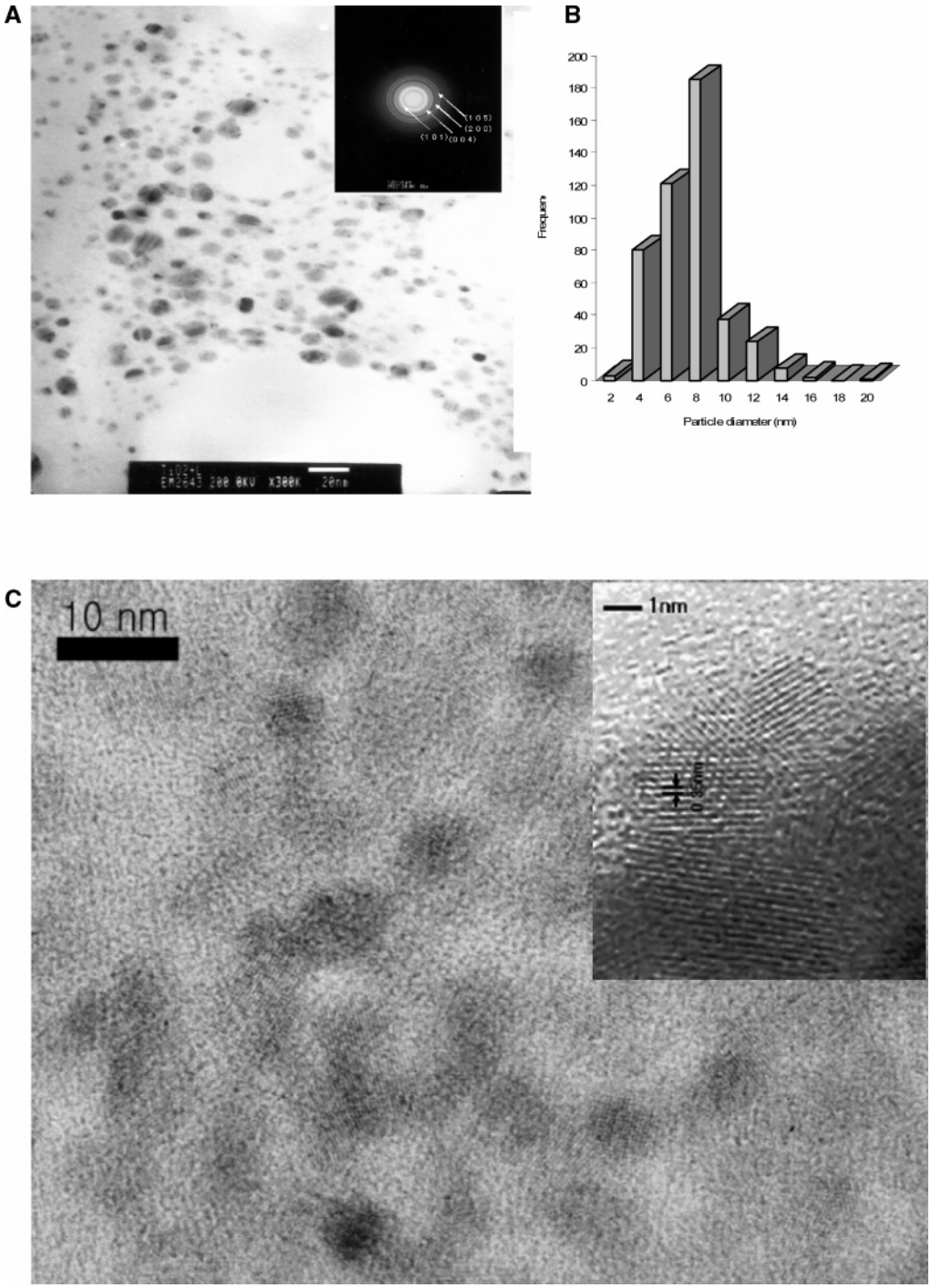

Figure 3. (A) TEM image of titania nanospherical particles. Inset: Selected area electrondiffraction pattern. (B) Size distribution of the nanospherical particles, exhibiting an average diameter of 9 nm. (C) High-resolution TEM image showing the lattice image of titania nanospherical particles (lattice spacing ~0.35 nm).

cm^{-1} in the region of 3200−4000 cm^{-1} is characteristic of OH groups weakly chemisorbed. In this region, additional vibrational bands with very weak fine structures were observed at 3750 and 3840 cm^{-1}, indicating the existence of relatively few octahedrally coordinated vacancies designated $_6Ti^{3+}$−OH in addition to tetrahedrally corrdinated vacancies designated $_4Ti^{4+}$−OH in contrast to the case of other TiO_2 nanoparticles,[28] implying that the surface structure is mostly in the form of TiO_2 with very little Ti_2O_3 on the titania nanodisk. It is quite interesting to note that two new vibrational bands were observed around 1094 and 1630 cm^{-1} which are not observed in the TiO_2 nanoparticles. The 1094 and 1630 cm^{-1} bands are attributed to Ti−O−H deformation and H−O−H bending vibrations, respectively,[29] indicating that the nanodisk is composed of Ti, O, and H. The surface structure formation of the titania nanodisk is unambiguously understood at present, but the FT-IR spectral results suggest

(27) Kumar, P. M.; Badrinarayanan, S.; Sastry, M. *Thin Solid Films* **2000**, *358*, 122.

(28) Dokhale, P. A.; Sali, N. D.; Madhu, P. *Mater. Sci. Eng., B* **1997**, *49*, 18.

(29) Bezrodna, T.; Puchkovska, G.; Shymanovska, V.; Baran, J.; Ratajczak, H. *J. Mol. Struct.* **2004**, *700*, 175.

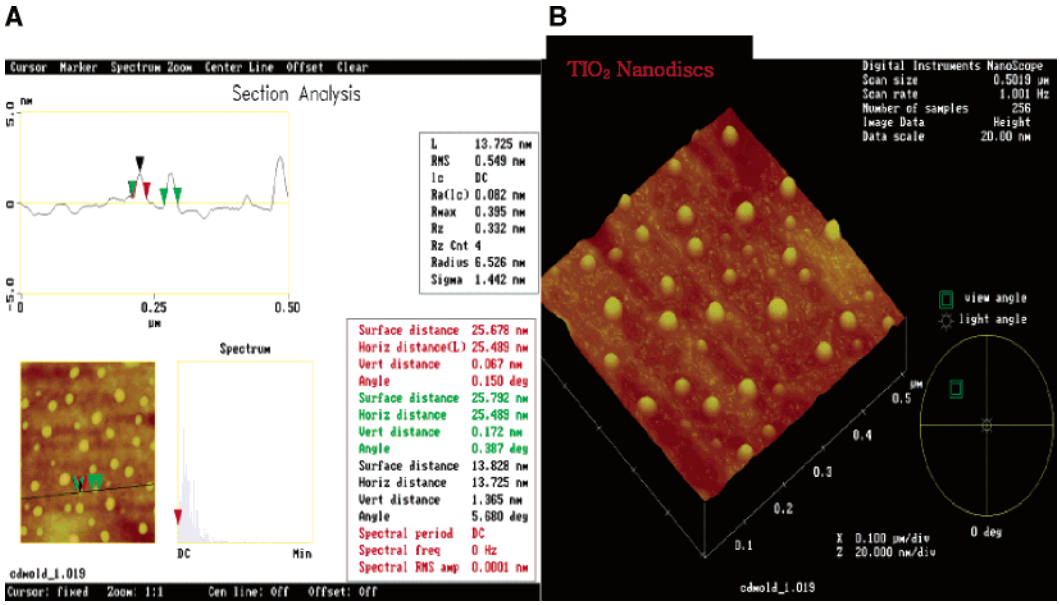

Figure 4. Tapping-mode AFM image (500 × 500 nm^2) of titania nanospherical particles obtained by calcination of the liposome−TiO_2 nanocomposites on quartz, (A) 2D and (B) 3D, exhibiting nanodisk morphology.

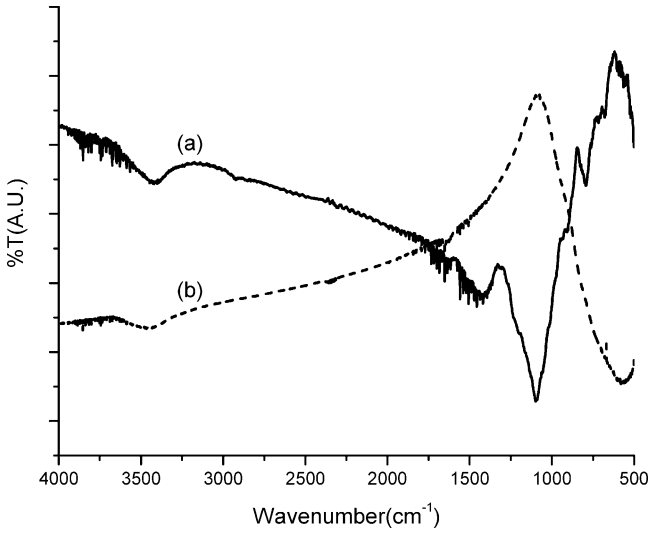

Figure 5. FT-IR spectra of (a) titania nanodisks and (b) TiO_2 nanoparticles.

that the $_4Ti^{4+}$−OH surface groups of the titania nanodisk are strongly H-bonded with chemisorbed water molecules as well as neighboring anions of the TiO_2 lattice and adjacent OH groups as follows. This is in agreement with the XPS data analysis discussed below.

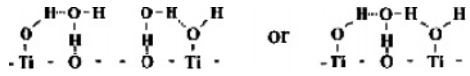

Figure 6 shows the XPS spectra of Ti 2p and O 1s core levels recorded from a pellet of titania nanodisk powder. The XPS peaks were assumed to have Gaussian line shapes and were resolved into individual components by a nonlinear least-squares procedure after proper subtraction of the baseline. Thus, the Ti 2p spectrum (Figure 6A) could be resolved into six spin−orbit components at binding energies of 457.75, 458.95, 460, 461.60, 426.95, and 464.75 eV, which are attributed to Ti^{3+} $2p_{3/2}$, Ti^{4+} $2p_{3/2}$, Ti^0 $2p_{1/2}$, Ti^{2+} $2p_{1/2}$, Ti^{3+} $2p_{1/2}$, and Ti^{4+} $2p_{1/2}$ species, respectively.[30] It is seen that the peak intensities for the Ti^{4+} $2p_{3/2}$ and Ti^{4+} $2p_{1/2}$ levels are significantly the largest as compared to those for other species, indicating that the dominant surface state of titania nanodisks consists of Ti^{4+} with a relatively lesser

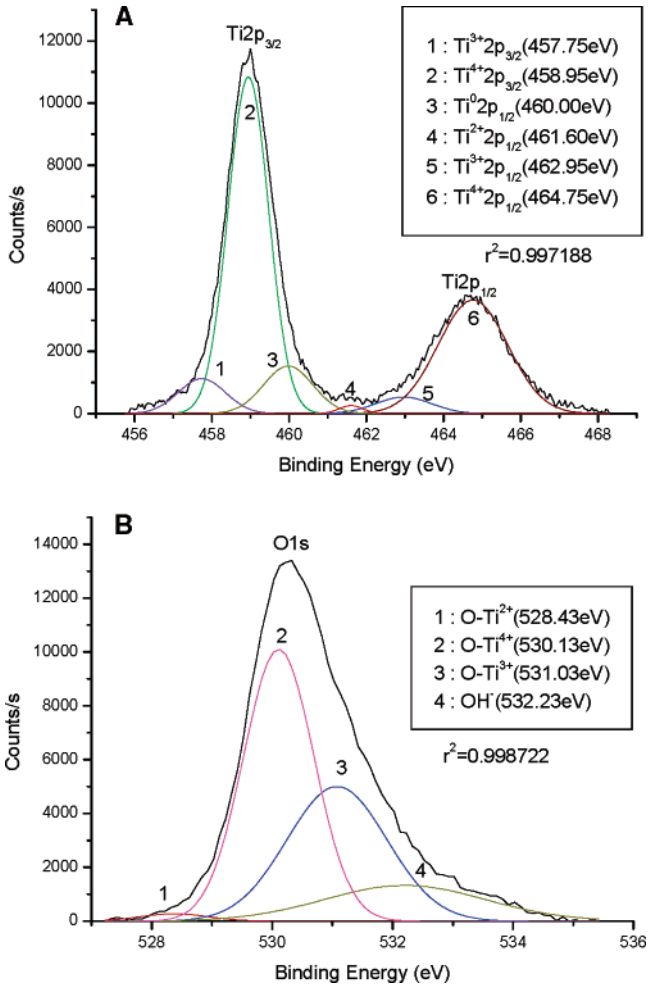

Figure 6. X-ray photoelectron spectra of the titania nanodisk surface at an electron takeoff angle of 55° together with the decomposition (see the text for details): (A) Ti $2p_{3/2,1/2}$ core level, (B) O 1s core level. r^2 stands for the fitting correlation coefficient.

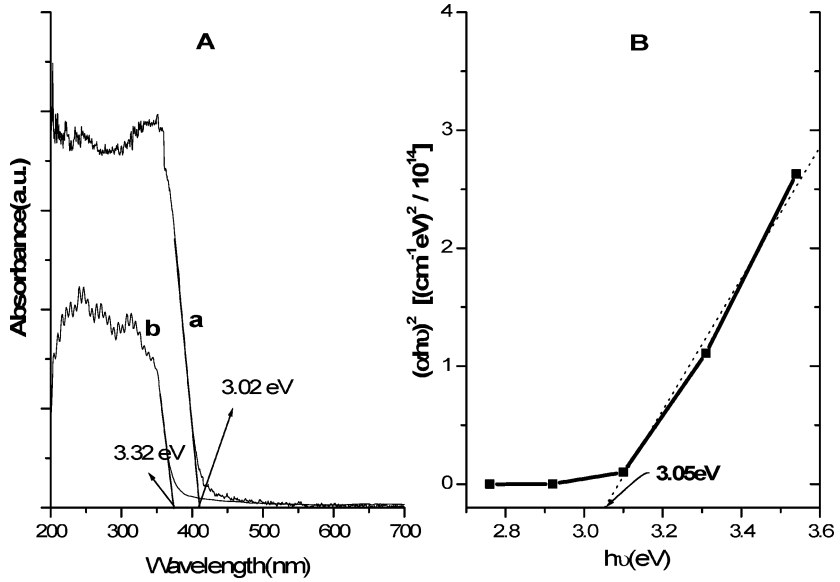

Figure 7. (A) Diffuse reflectance absorption spectrum of (a) titania nanodisks and (b) TiO_2 nanoparticles. (B) Variation of $(\alpha h\nu)^2$ with the absorption energy ($h\nu$) for titania nanodisks to identify an indirect transition.

extent of Ti^{3+}, a coordinatively unsaturated ion in contrast to that of other TiO_2 nanoparticles,[27] being in agreement with the FT-IR results. In parallel with this, the resolved O 1s spectrum (Figure 6B) also exhibits the larger intensity of $O-Ti^{4+}$ at 530.13 eV as compared to that of $O-Ti^{3+}$ at 531.03 eV, in agreement with the previous work.[30] It is also interesting to note that the chemisorbed OH species could be observed at high binding energy, 532.23 eV, as demonstrated by previous works.[27,30] These results again suggest that the $-OH$ group is chemisorbed on the Ti sites as mostly Ti^{4+} sites alternatively with H_2O as discussed from the FT-IR results.

Optical Properties. Figure 7A shows the diffuse reflectance UV−vis absorption spectrum of titania nanodisks (curve a) along with that of TiO_2 nanoparticle dots prepared by hydrolysis (curve b). It shows a steep rise in absorbance from the absorption edge at 410 nm to the absorption maximum around 370 nm attributed to the interband transition. It also exhibits a weak but significantly broadened band at longer wavelengths than 400 nm below the absorption edge as compared with that of bulk TiO_2. This indicates the presence of surface states for the electronic transition as observed in ZnS nanoparticles.[31]

The onset of absorption of the titania nanodisks is extrapolated to 3.02 eV corresponding to the band-gap energy, which is significantly lower as compared to that of the nanodisk's precursor, TiO_2 nanoparticles (3.32 eV). To determine the nature of the band gap, either an indirect or a direct transition, the following power expression for the variation of the absorption coefficient (α) with energy was examined:[32,33]

$$(\alpha h\nu)^n = k_{i,d}(h\nu - E_g)$$

where $k_{i,d}$ is the absorption constant for an indirect (subscript i) or direct (subscript d) transition, n is 2 for an indirect transition and 1/2 for a direct transition, $h\nu$ is the absorption energy, and E_g is the band-gap energy. The absorption coefficient (α, cm^{-1}) was determined from the equation $\alpha = (2.303 \times 10^3)(A\rho/lc)$ by using the measured absorbance (A), density (ρ, 3.89 g/cm^3 for anatase), optical path length (l) (1 cm), and concentration of TiO_2 (c, 1.25 g/L). Variation of $(\alpha h\nu)^2$ with absorption energy ($h\nu$) for titania nanodisks (Figure 7B) gives the extrapolated intercept corresponding to the band-gap energy at 3.05 eV, which is close to the onset energy observed in the absorption spectrum, confirming that the band gap is attributed to the indirect transition. The indirect transition is convincingly shown in the PL spectroscopic studies (vide infra). This is in contrast to the direct electronic transition dominant for the band gap of the TiO_2 crystalline nanoparticle,[24,27] implying that interaction between the exciton and lattice phonon on the surface of titania nanodisks is stronger than that of the simple TiO_2 crystalline nanoparticle.[34]

Figure 8 shows the PL emission and excitation spectra of titania nanodisks measured at ambient temperature. The PL emission spectrum was observed with excitation at 360 nm, exhibiting a strong structural emission band around 425 nm with broad shoulders beyond 460 nm down to 600 nm. The PL excitation spectrum was measured with the 440 nm emission. Crossing of the PL emission and excitation spectra was observed to show the 0−0 transition at 410 nm, which matched well with the band-gap energy (3.02 eV) as determined from the absorption spectra. The PL excitation spectrum showed a stronger excitation band at a lower region (around 400 nm) than at a higher energy region in contrast to the absorption spectral feature, supporting the prediction of the presence of surface states as aforementioned. It should also be noteworthy that at higher energy excitation (280 nm)

(30) Pouilleau, J.; Devilliers, D.; Groult, H.; Marcus, P. *J. Mater. Sci.* **1997**, *32*, 5645.
(31) Chen, W.; Wang, Z.; Lin, Z.; Lin, L. *J. Appl. Phys.* **1997**, *82*, 3111.
(32) Zhao, X. K.; Fendler, J. H. *J. Phys. Chem.* **1991**, *95*, 3716.
(33) Monticone, S.; Tufeu, R.; Kanaev, A. V.; Scolan, E.; Sanchez, C. *Appl. Surf. Sci.* **2000**, *162*, 565.
(34) Kimov, V. I. Linear and Nonlinear Optical Spectroscopy of Semiconductor Nanocrystals. In *Handbook of Nanostructured Materials and Nanotechnology*; Nalwa, H. S., Ed.; 2000; Vol. 4: Optical Properties, Chapter 7.

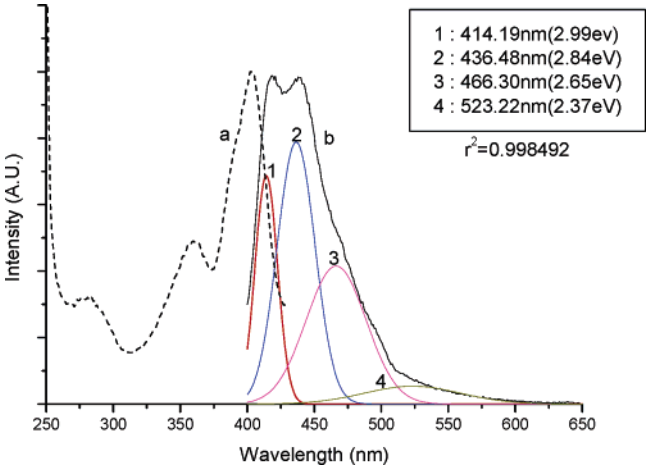

Figure 8. PL excitation (a) and emission (b) spectra of titania nanodisks at ambient temperature. The excitation wavelength for emission was 360 nm, and the emission wavelength for the excitation spectrum was 440 nm. The PL emission spectrum was resolved into four different individual bands by using the nonlinear least-squares method based on the Gaussian line shape.

an additional weak emission was observed near 350 nm (data not shown). This excitation-energy dependence of the emission is similar to that observed for the surface emission of 2.38 nm for CdS nanoclusters having a narrow size distribution and a large BET specific surface area.[35] Therefore, the strong emission in the region of 410−600 nm is assigned to the surface-state emission originating from the recombination of a hole with an electron trapped on the surface state, whereas the weak additional 350 nm emission observed by higher energy excitation is just a band-edge emission originating from the interband transition. Actually, at the higher excitation energy, the hole wave function is known to be located at the center of the nanocluster and has good overlap with the electron wave function,[36] and the recombination of the electron−hole pair is too fast to be observed. However, when the charge carriers are trapped on the surface states, the hole and the electron are localized so that spatial overlap of the charge carriers is reduced to retard the recombination of the charge carriers.[37] This is why the surface emission is very strong but the band-edge emission is weak, implying that the titania nanodisks with a large BET specific surface area have abundant surface states as compared to the simple nanoparticle dots.

The PL excitation spectrum (Figure 8a) of the titania nanodisks also exhibited an excitation band around 280 nm which is close to the inhomogeneous absorption maximum bands (Figure 7), not otherwise observed for the liposome−TiO_2 nanocomposites for which the surface states of titania are passivated, indicating that the surface energy levels for the excitons to be trapped on the titania nanodisks are widely dispersed. In fact, the PL emission band was assumed to have Gaussian line shapes and could be analyzed to be composed of four different emission bands at 2.99, 2.84, 2.65, and 2.37 eV, by using nonlinear least-squares methods. These energy levels can be assigned to various transitions on the basis of the transition energy diagrams of TiO_2 particles calculated by Daude et al.[37] as shown in Table 1. As in the case of TiO_2 nanoparticle dots, the 2.65 and 2.37 eV bands are 1.37−1.65 eV below the band-gap energy (3.02 eV), and they should correspond to the energy of the deep-trap surface state. These energy values are similar to several defect energy levels of TiO_2 nanoparticles detected by Ghosh et al.,[38] and they are attributed mostly to Ti^{4+} ions adjacent to oxygen vacancies with a few coordinatively unsaturated ions (cus), Ti^{3+} incorporated with OH as observed from FT-IR data. However, the maximum PL signals at 2.99 and 2.84 eV are close to the band-gap energy, and they should originate from the charge recombination on the shallow-trap surface state. It is also interesting to note that the shallow-trap emissions are exclusively attributed to the indirect transition as seen in Table 1. This observation is consistent with that of the indirect transition observed from the absorption spectral data. This is quite in contrast to the case of TiO_2 crystalline nanoparticles which show surface PL ascribed to the direct transition dominantly with a small portion of the indirect transition,[24] indicating that the exciton interactions with the lattice phonon in the titania nanospheres are relatively stronger as compared to those of TiO_2 nanoparticle dots.[37] Because of the strong coupling of the wave functions of the trapped electrons or holes with the lattice phonons of the nanostructures, the dominant decay route for the initially generated excitons in the nanostructures would be a nonradiative path, such as relaxation to another surface state.[39]

Table 1. Energy Levels of Titania Nanospheres Corresponding to the Various Types of Transitions Assigned According to the Energy Level Diagram Calculated by Daude et al.[37]

transition	nature	energy (±0.03, eV)
$X_{2b} \rightarrow \Gamma_{1b}$	indirect	3.02
$X_{1a} \rightarrow \Gamma_{1b}$	indirect	2.99, 2.84
defect levels/oxygen vacancies		2.65, 2.37

To further study the PL spectroscopic properties related to the recombination dynamics of the photogenerated charge carriers, the PL decay times were measured by using a femtosecond Ti:sapphire laser attached to TCSPC detectors. Figure 9 shows the typical PL decay profiles of three different surface emissions (406, 440, and 520 nm) of the titania nanodisks measured by excitation with a 364 nm laser (1.2 μW/pulse), which were analyzed to be triexponential. Their decay time constants are listed in Table 2. Generally, the amplitudes of the decay time constants depend on the emission wavelengths, indicating that the PL spectrum consists of more than three different surface emissions as discussed above. For the 406 nm emission, the fast decay time (21 ps) is dominant (52%) with a small portion of two slower decay components (1.44 and 4.31 ns), but its amplitude is significantly decreased for the 440 and 520 nm emissions. This implies that the fast decay is ascribed to the radiative recombination of the charge carriers trapped on the band-edge state, since 406 nm is close to the band-gap energy as in the case of TiO_2 nanoparticle dots.[24] For the 440 nm

(35) Skinner, D. E.; Colombo, P., Jr.; Cavaleri, J. J.; Bowman, R. M. *J. Phys. Chem.* **1995**, *99*, 7853.
(36) Wang, Y.; Herron, N. *J. Phys. Chem.* **1991**, *95*, 525.
(37) Daude, N.; Gout, C.; Jouanin, C. *Phys. Rev. B* **1977**, *15*, 3229.
(38) Ramakrishna, G.; Das, A.; Ghosh, H. N. *Langmuir* **2004**, *20*, 1430.
(39) Graetzel, M. *Heterogeneous Photochemical Electron Transfer*; CRC Press: Boca Raton, FL, 1989.

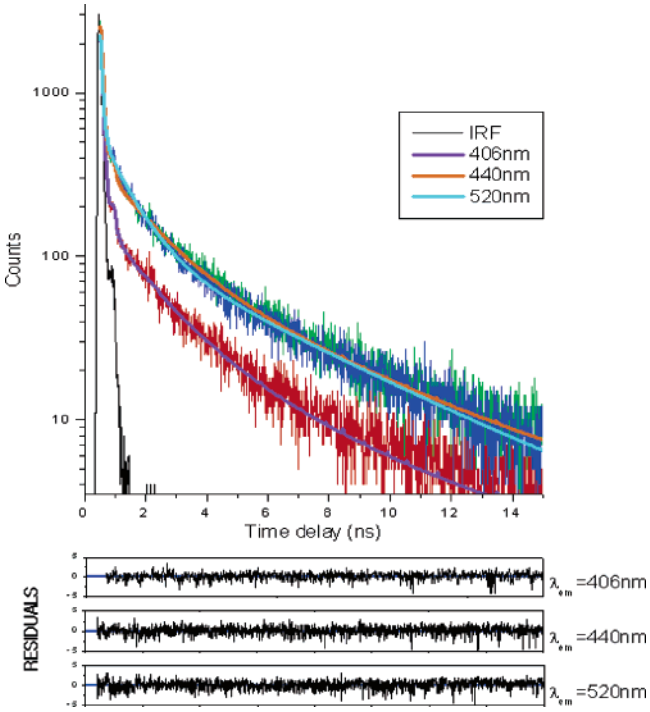

Figure 9. PL decay time profile of titania nanodisks. The excitation wavelength is 364 nm, and the monitoring wavelength is 460 nm. The panel at the bottom is the PL decay time profile of liposome−TiO_2 nanocomposites.

Table 2. PL Decay Times of Titania Nanodisks Measured at Three Different Emission Wavelengths

λ_{em} (nm)	amp1 (%)	τ_1 (ps)	amp2 (%)	τ_2 (ns)	amp3 (%)	τ_3 (ns)	χ^2
406	52	21	24	1.44	24	4.31	1.030
440	38	37	27	1.48	35	4.95	1.123
520	24.	22	35	1.13	41	5.62	1.112

emission, the amplitudes of the slower decay time components (1.48 and 4.95 ns) were observed to be significantly increased as compared with those observed from the 406 nm emission. The amplitudes of these slower decay components were observed to be further increased for the 520 nm emission, even though their decay times (1.13 and 5.62 ns) were somewhat different from those observed from the 406 or 440 nm emission. The difference in the slower decay times may be due to the widely dispersed surface states or size distribution of titania nanodisks, but it is difficult to distinguish these two possibilities under the present data obtained by ensemble-averaged spectroscopic techniques. Nevertheless, on the basis of the emission wavelength dependence of the amplitudes of the decay components, it seems to be clear that the slower decay components are attributed to the emission from the lower energy states of titania nanodisks such as shallow-trap or deep-trap surface states. As a comparison, the decay times of the 440 nm emission from the liposome−TiO_2 nanocomposites were measured, and they were determined to be 69 ps (75%) and 1.56 ns (25%) without observation of the slowest decay component (4.95 or 5.62 ns) of titania nanodisks. In the liposome−TiO_2 nanocomposites the defect surface with oxygen vacancies of TiO_2 as the deep-trap surface site is passivated by interaction with lipid, and the emission component originating from the excitons on the deep-trap

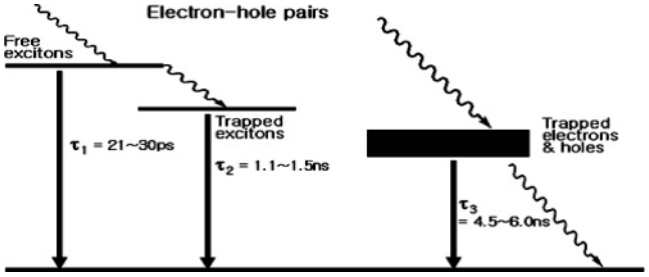

Figure 10. A proposed model of recombination dynamics of charge carriers on the surface of titania nanodisks. The curly arrows represent the nonradiative recombination processes.

surface state is not efficiently observed. Therefore, the slowest decay component of the emission from the titania nanospheres should originate from the deep-trap surface as observed from the steady-state PL studies.

According to the steady-state and time-resolved spectroscopic results, the recombination dynamics of the photogenerated charge carriers can be illustrated briefly by the energy diagram shown in Figure 10. The incoming photons result in formation of a free electron and hole on the conduction band and valence band, respectively, and a part of the photogenerated charge carriers recombine radiatively in the band-edge state very quickly within 20−30 ps. Another part of them relax to the surface to be trapped on shallow-trap surface states which consequently recombine radiatively with a lifetime of 1.1−1.5 ns. In parallel, some of the photogenerated charge carriers could be trapped into the deep-trap center and consequently recombine radiatively with a much longer lifetime of 4.5−6.0 ns. This trapping process should be due to the strong interaction of the excitons with the lattice phonon of the nanostructures as discussed above. The long decay time constants of the deep-trap emission were also expected in the TiO_2 nanoparticle dots, but they have not been measured practically, implying that the population of the deep-trap surface states is relatively low in the TiO_2 nanoparticle dots. Therefore, the successful observation of the long decay time constants suggests that the population of the deep-trap surface states is much higher in the titania nanodisks than in the TiO_2 nanoparticle dots. The slower decay times of the deep-trap emission reflect that the charge-carrier recombination is significantly prolonged in the deep-trap surface state of the titania nanodisks.

Photocatalytic Activities. The prolonged recombination of the surface charge carriers implies that the titania nanodisks would be very useful as highly improved photoelectric functional materials such as photocatalysts and solar cells. To confirm this implication, we attempted to observe the photocatalytic activities of the titania nanodisks by monitoring the photoreduction and photooxidation of MO (5.0×10^{-6} M) in aqueous solution under argon gas and oxygen bubbling, respectively. Figure 11A shows the UV−vis spectra of a 10 mL MO solution measured as a function of irradiation with light (>320 nm) in the presence of 5 mg of titania nanodisks under argon gas bubbling. MO itself in the absence of titania nanodisks was photochemically inert as observed by no change in the absorption spectrum upon irradiation. However, in the presence of the nanodisks, the absorption spectrum was significantly changed. The visible

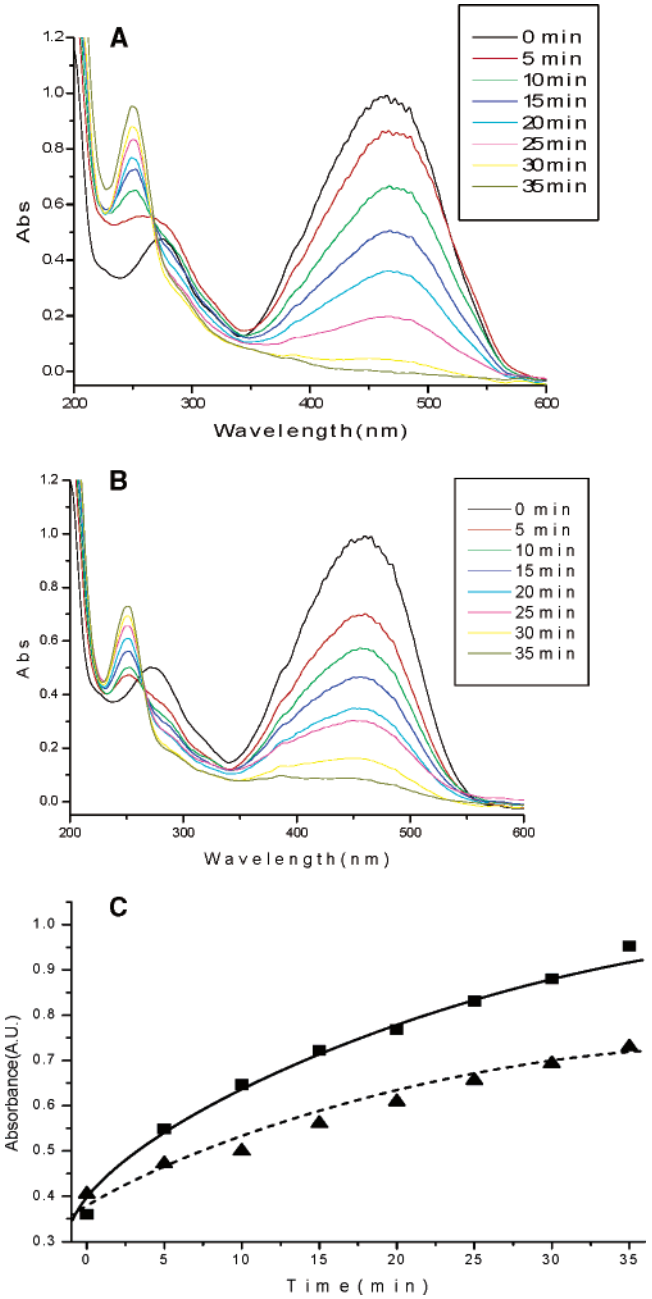

Figure 11. Absorption spectral changes of the filtered solution of MO after irradiation in the presence of (A) titania nanodisks and (B) P-25. (C) Absorption change of MO at 250 nm corresponding to formation of hydrazine as a function of the irradiation time (■, titania nanodisks; ▲, P-25).

absorption band around 475 nm decreases, and a new peak grows up at 250 nm which originates from a reduction product, hydrazine.[40] The spectral change was completed in 30 min. This indicates that photoreduction of MO is well catalyzed by titania nanodisks through electron transfer as shown in the following reaction: $(CH_3)_2NC_6H_4N{=}NC_6H_4SO^{3-}$ (MO) $+ 2H^+ + 2e^- \rightarrow (CH_3)_2NC_6H_4NHNHC_6H_4SO^{3-}$ (hydrazine). The same spectral change of the 10 mL MO solution was also observed in the presence of 5 mg of Degussa P-25 titania under the same irradiation condition as that carried out in the presence of titania nanodisks, but the spectral change took a little longer as shown in Figure 11B. Figure 11C shows a plot of the degree of photoreduction monitored by formation of hydrazine in the presence of titania nanodisks and Degussa P-25 as a function of the irradiation time. This shows that the photocatalytic reduction of MO is 5 times faster in the presence of titania nanodisks than in the presence of Degussa P-25. The quantum efficiency of photocatalytic reduction was determined by calculating the number of moles of hydrazine formed by 30 min of irradiation with 320 nm light (photonic output of the lamp 9.7×10^{-9} einstein/min). Thus, the quantum efficiency of the photocatalytic reduction of titania nanodisks was found to be much higher ($\Phi_{ND} = 0.38$) than that of Degussa P-25 ($\Phi_{P-25} = 0.24$).

The photocatalytic oxidation of MO (5.0×10^{-6} M) in aerobic aqueous solution containing 5 mg of titania nanodisks was also observed by monitoring its absorption spectral change as reported earlier,[41,42] which exhibited ca. 90% destruction of the absorption maximum band at 465 nm with a new species detected at ca. 410 nm upon 45 min of irradiation. The new species was observed to completely disappear upon a further 15 min of irradiation, indicating that MO is completely destructed into CO_2 and H_2O. However, upon irradiation of the aqueous solution of MO in the presence of P-25, only the intensity of the 465 nm band was decreased without the new species detected at the slower rate as compared to that observed in the presence of titania nanodisks, and no further destruction of the spectrum was observed within 60 min of irradiation. These observations indicate that the photocatalytic efficiency of titania nanodisks for photooxidation is also significantly higher than that of P-25.

Conclusion

New one-dimensional titania nanostructures were synthesized by formation of egg lecithin liposome−TiO_2 nanocomposites, which were identified to be single-crystalline anatase nanodisks with an average diameter of 9 nm and height of 0.5 nm. Their BET specific surface area (227 g/m^2) is much larger than that of TiO_2 nanopaticle dots of the same diameter. Their band-gap energy was observed to be red-shifted (3.02 eV) as compared to that of TiO_2 nanopaticle dots. The UV−vis absorption and the fluorescence emission spectral data demonstrated that the indirect transition is the exclusive route for charge-carrier recombination, indicating the strong coupling of wave functions of the trapped exciton pair with lattice phonons. The femtosecond laser time-resolved fluorescence measurements exhibited three emissive decay components (~22 ps, 1.1−1.5 ns, 4.5−6.0 ns). Depending on the emission wavelength, the slower decay times were somewhat different probably due to the widely dispersed surface states or size distribution of the titania nanodisks. This wavelength dependence is now under scrutinization by using the single-molecule spectroscopic technique. Nevertheless, on the basis of the emission wavelength dependence of the amplitudes of the decay components, it seems to be clear that the slower decay components are attributed to the emission from the lower energy states of titania nanodisks such as shallow-trap or deep-trap surface states. The longest decay

(40) Brown, G. T.; Darwent, J. R. *J. Chem Soc., Faraday Trans. 1* **1984**, *80*, 1631.
(41) Brown, G. T.; Darwent, J. R. *J. Phys. Chem.* **1984**, *88*, 4955.
(42) Al-Qaradawi, S.; Salman, S. R. *J. Photochem. Photobiol., A* **2002**, *148*, 161.

component (4.5−6.0 ns), which is not observed from titania nanoparticle dots, implies the possibility of application of the titania nanodisks to develop a highly efficient photocatalyst, solar cell, or photoelectronic device as confirmed by the high photocatalytic quantum efficiency of photoreduction of MO.

Acknowledgment. This work has been financially supported by the Korea Science and Engineering Foundation through the Joint Research Project under the Korea-Japan Basic Scientific Cooperation Program (KOSEF Grant F01-2004-000-10024-0).

CM0515855